

SimBEV: A Synthetic Multi-Task Multi-Sensor Driving Data Generation Tool and Dataset

Goodarz Mehr* Azim Eskandarian
Virginia Commonwealth University

{mehrg, eskandariana}@vcu.edu

<https://github.com/GoodarzMehr/SimBEV>

Abstract

Bird’s-eye view (BEV) perception for autonomous driving has garnered significant attention in recent years, in part because BEV representation facilitates the fusion of multi-sensor data. This enables a variety of perception tasks including BEV segmentation, a concise view of the environment that can be used to plan a vehicle’s trajectory. However, this representation is not fully supported by existing datasets, and creation of new datasets can be a time-consuming endeavor. To address this problem, in this paper we introduce SimBEV, an extensively configurable and scalable randomized synthetic data generation tool that incorporates information from multiple sources to capture accurate BEV ground truth data, supports a comprehensive array of sensors, and enables a variety of perception tasks including BEV segmentation and 3D object detection. We use SimBEV to create the SimBEV dataset, a large collection of annotated perception data from diverse driving scenarios.

1. Introduction

Autonomous driving promises a future with safer, cleaner, more efficient, and more reliable transportation systems [11, 58]. As the development of autonomous vehicle technology has accelerated in recent years, so has the need for perception algorithms capable of understanding complex driving scenarios in diverse environments [7, 73]. High-quality driving datasets have been at the center of the recent progress, serving as a foundation for training and benchmarking novel perception algorithms. It is essential for such datasets to encompass a large variety of driving scenarios and encapsulate a diverse set of road types, weather conditions, and traffic patterns, so perception models can effectively generalize to real-world situations [15, 32, 53].

As essential in this context is multimodal sensor fusion, which plays an important role in enhancing the performance

of perception algorithms by compensating for weaknesses of one modality with the strengths of others [5, 67, 77]. Sensor fusion improves an autonomous vehicle’s understanding of its surrounding environment [59] (especially in adverse weather conditions [1]), enables robust decision-making in dynamic scenarios [19, 50], and opens the door to perception models that can accomplish multiple tasks simultaneously [20, 35, 43, 47]. Consequently, it is imperative for driving datasets to support a wide array of sensors and various computer vision tasks (such as object detection, semantic segmentation, and tracking) to facilitate the development of multi-faceted perception systems that leverage the strength of multiple sensing modalities.

Bird’s-eye view (BEV) perception has garnered significant attention in recent years for two primary reasons [40]. First, BEV representation is conducive to the fusion of information from different modalities, perspectives, and agents, and extracted BEV features can be used for various perception tasks. Second, BEV segmentation offers a concise, geometrically accurate and semantically rich view of the surrounding environment that can be directly used by motion planning, behavior prediction, and control algorithms. These two factors have given rise to perception algorithms that utilize BEV representation for 3D object detection, BEV segmentation, or both [3, 10, 13, 14, 17, 20, 21, 23, 25–28, 30, 33, 35, 36, 39, 41, 42, 45, 57, 60, 61, 64–66, 69, 70, 72, 74, 75].

However, despite the growing interest in BEV perception, few existing datasets support BEV segmentation. In the ones that do, either the BEV ground truth is limited to static map elements (drivable area, pedestrian crossing, etc.) [2], or BEV ground truth is only provided for a small window around the ego vehicle, obtained through combining map elements with select 3D object bounding boxes [16].

Creating a new dataset to address this gap is a challenging, time-consuming, and resource-intensive endeavor. Real-world driving data has to be collected over a long period of time to ensure weather conditions and traffic patterns present in the dataset are diverse, and requires (at least

*Work partially done while at Virginia Tech.

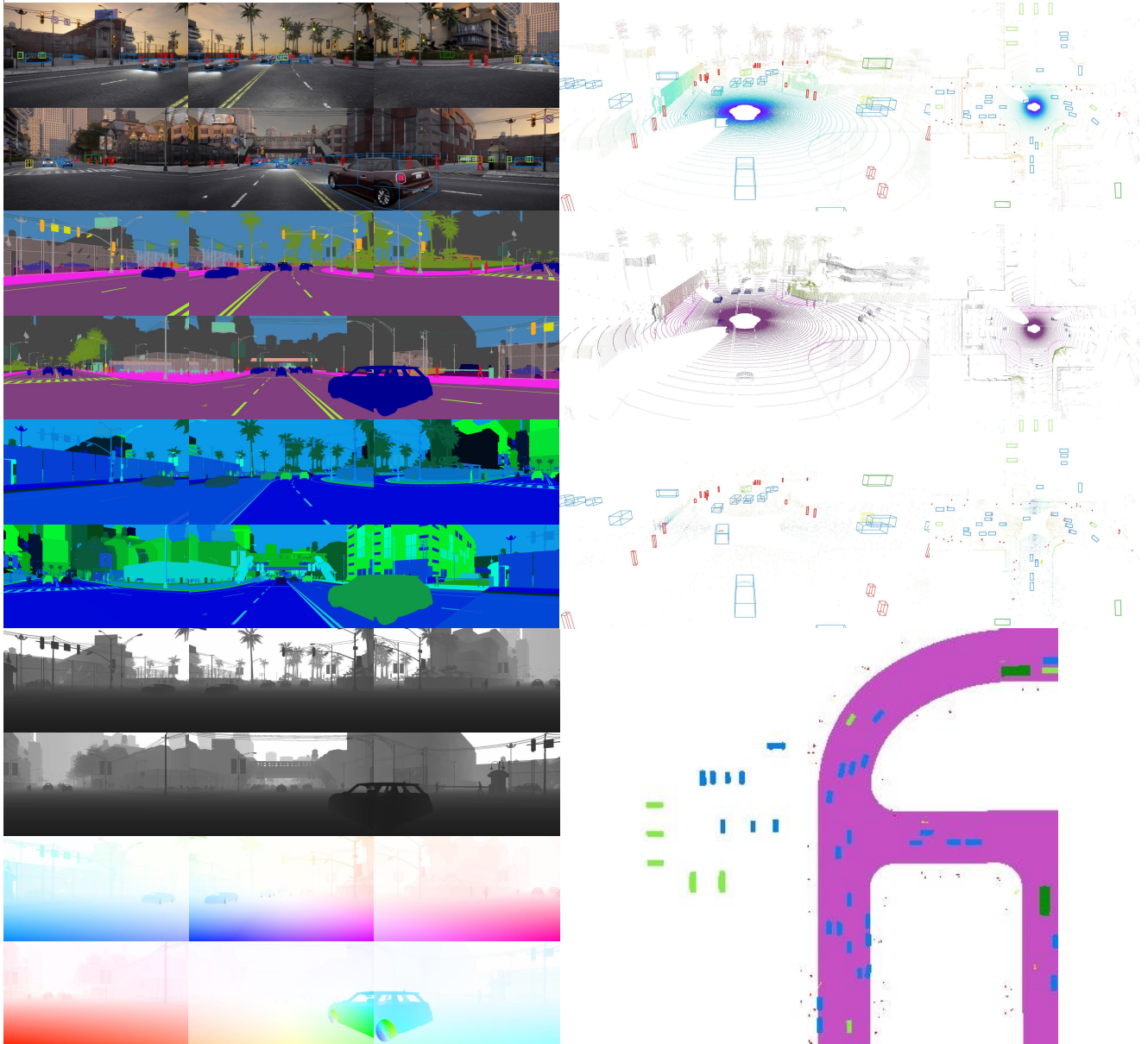


Figure 1. A data sample generated by SimBEV. The left half depicts a 360-degree view of the ego vehicle’s surroundings using different camera types (from top to bottom RGB, semantic segmentation, instance segmentation, depth, and optical flow cameras, respectively). On the right half, views of lidar, semantic lidar, radar, and the BEV ground truth are shown from top to bottom, respectively. Some images also contain 3D object bounding boxes.

partly) labor-intensive hand annotation [32, 56]. As for synthetic datasets, they often consist of carefully designed scenarios that may not capture the full diversity of the driving environment, and may not be as challenging for perception algorithms as their creators think they are. Aside from all this, simply getting an overhead view of the ego vehicle in either case may not result in an accurate BEV ground truth due to the presence of vegetation and other structures (traffic lights, bridges, etc.) that obstruct the overhead view [31].

To overcome these challenges, our paper makes two

main contributions. First, we introduce SimBEV, an extensively configurable and scalable randomized synthetic data generation tool that incorporates information from multiple sources to capture accurate BEV ground truth data. In addition to diverse driving scenarios, SimBEV also provides 3D object bounding boxes and supports a variety of configurable perception and localization sensors. This makes it an invaluable tool for empowering researchers to explore various computer vision tasks, and ultimately, accelerate the development of more capable and resilient autonomous driv-

	Dataset	Year	Scenes	Annotated frames	2D Det	3D Det	2D Seg	3D Seg	BEV Seg
Real-world	KITTI [12]	2012	22	41K	✓	✓	-	-	-
	Cityscapes [6]	2016	-	25K	✓	✓	✓	-	-
	Mapillary [44]	2017	-	25K	-	-	✓	-	-
	ApolloScape [18]	2018	103	144K	✓	✓	✓	✓	-
	Argoverse [4]	2019	113	22K	✓	✓	-	-	limited
	Waymo Open [54]	2019	1150	230K	✓	✓	✓	-	-
	nuScenes [2]	2019	1000	40K	✓	✓	✓	✓	limited
	A*3D [46]	2020	-	39K	-	✓	-	-	-
	BDD100K [71]	2020	100K	12M	✓	-	✓	-	limited
	Lyft Level 5 [16]	2021	366	46K	-	✓	-	-	limited
Argoverse 2 [63]	2021	1000	6M	✓	✓	-	-	limited	
Synthetic	SYNTHIA [49]	2016	-	13K	✓	✓	✓	-	-
	GTA-V [48]	2016	-	25K	-	-	✓	-	-
	ViPER [51]	2017	-	254K	✓	✓	✓	-	-
	All-in-One Drive [62]	2021	100	100K	✓	✓	✓	✓	-
	SHIFT [55]	2022	4850	2.5M	✓	✓	✓	-	-
	SimBEV	2024	320	102K	✓	✓	✓	✓	✓

Table 1. Comparison of the size and supported tasks of the most notable existing single-vehicle driving datasets. SimBEV is the only dataset that provides full support for BEV perception.

ing systems. Second, we use SimBEV to create the SimBEV dataset, a comprehensive large-scale dataset that can serve as a benchmark for a variety of perception tasks and have applications beyond it. One data sample generated by SimBEV is shown in Fig. 1.

2. Related Work

Real-world driving datasets generally target specific subsets of perception tasks, as the high costs associated with data collection and labeling limit their scope. One of the most prominent and oldest driving datasets is the KITTI dataset [12], which supports depth estimation and 2D and 3D object detection and tracking. Other notable image-based datasets include Cityscapes [6], and Mapillary [44], which are geared towards segmentation, while A*3D [46] focuses on 3D object detection. More recently, large-scale datasets such as BDD100K [71], Waymo Open [54], ApolloScape [18], Argoverse 2 [63], and nuScenes [2] have emerged, offering multi-modal data and multi-task annotations but primarily emphasizing object detection and tracking.

Synthetic driving datasets are compiled using graphics engines and physics simulators. For instance, SYNTHIA [49] incorporates RGB and semantically segmented images generated by its dedicated simulator. Video games have also served as a source of data. For example, GTA-V [48] offers RGB and semantically segmented images extracted from GTA. ViPER [51] expands upon it by including optical flow images and discrete environmental labels. The introduction of CARLA (CAR Learning to Act) Simulator [9], built upon Unreal Engine 4 (UE4), enabled the systemic generation of driving datasets. All-in-One Drive [62] is one such dataset, featuring support for multiple sensors and a focus on SPAD (Single-Photon Avalanche Detector)-

lidars. Another notable dataset is the SHIFT dataset [55], a large-scale multi-task multi-modal synthetic dataset for autonomous driving, designed to simulate discrete and continuous shifts in weather and traffic conditions.

Existing datasets offer limited support for BEV segmentation. In nuScenes [2] BEV segmentation is only supported for static map elements (drivable area, lane line, pedestrian crossing, etc.). In Lyft Level 5 [16] and Argoverse 1 and 2 [4, 63], BEV ground truth is obtained through combining map elements and vehicle bounding boxes observable by the perception sensors, limiting BEV ground truth area and potentially missing some occluded objects.

Some vehicle-to-everything (V2X) datasets have support for BEV segmentation, but it is again limited. H-V2X [31] captures the BEV ground truth using overhead cameras installed along a 100 km highway, with the data limited to highway driving and mostly suitable for highway motion forecasting. The synthetic OPV2V [68] dataset provides BEV ground truth only for the drivable area, lane line, and vehicle classes, and the former can be inaccurate because it is calculated using waypoints only. Finally, the synthetic V2X-Sim [24] dataset captures the BEV ground truth using an overhead camera, limiting driving scenarios and causing inaccuracies due to vegetation, traffic light poles, and other structures that obstruct the overhead view.

3. SimBEV

SimBEV relies on a customized version of CARLA 0.9.15 [9] (see the Supplementary Material) to simulate the environment, perception sensors, and traffic behavior, although it is compatible with the standard release of CARLA as well. In the following, we describe how SimBEV operates and generates driving data.

3.1. Design

Instead of using carefully crafted scenarios, designing which can be very time-consuming, SimBEV relies on randomizing as many simulation parameters as possible to quickly create a statistically diverse set of scenarios. To create a new dataset, SimBEV generates and collects data from consecutive episodes, or scenes.

To start, the user configures the desired number of scenes for each map (i.e. driving environment, can be an existing CARLA map or a custom one) for each of the training, validation, and test sets. SimBEV checks to see if a SimBEV dataset already exists. If it does, SimBEV subtracts the number of existing scenes in that dataset from the number of desired scenes for each map. This feature allows the user to expand an already existing SimBEV dataset, or to continue with dataset creation in the event of a crash. SimBEV also allows the user to replace individual scenes.

At the start of each scene, SimBEV creates uniformly distributed waypoints within a certain distance of each other (specified by the user, 24.0 m by default) across the map's roads and selects one at random to use to spawn the ego vehicle and the desired perception and localization sensors attached to it, though the user also has the option to specify a set of spawn points that SimBEV can choose from. SimBEV then configures the weather at random and, if at night, changes the intensity of street lights randomly.

To create background traffic, SimBEV randomly chooses the desired number of background vehicles and pedestrians, although the user has the option to specify each. It then uses the waypoints mentioned previously to spawn random vehicles at random positions, and spawns pedestrians at random on walkable areas of the map. CARLA's traffic manager controls the behavior of vehicles and pedestrians throughout the episode.

Because all vehicles and pedestrians start from rest, SimBEV runs the simulation for a user-specified period of time (called warm-up duration, by default 4 s) before collecting data for a user-specified period of time (by default 16 s). During data collection, at each time step SimBEV collects and saves data from the desired sensors, and calculates and saves both 3D object bounding boxes and BEV ground truth masks. Following data collection, it saves meta-information about the data and a log of the scene, destroys the vehicles, pedestrians, and sensors, and starts a new scene.

3.2. Sensors

SimBEV supports a variety of sensors available in CARLA. They include five different camera types (RGB, semantic segmentation, instance segmentation, depth, and optical flow), two different lidar types (regular and semantic), radar, GNSS, and IMU, as shown in Fig. 1. The user has full control over each sensor's parameters (e.g. a camera's resolution or FoV), but the placement of the sensors is fixed

for now. The cameras are placed at six locations above the vehicle similar to [2] to offer a 360-degree view of the vehicle's surroundings, while a radar is placed on each side of the vehicle. GNSS and IMU sensors are placed at the center of the vehicle (the origin of the vehicle's coordinate system), while the lidar is placed high above that center.

3.3. Scene configuration

As discussed in what follows, numerous parameters are randomized for each scene to ensure that scenes are as unique and diverse as possible.

Weather. Weather in CARLA is configured using several parameters such as rain intensity, fog density, sun altitude angle, wind intensity, etc. By default, SimBEV randomly assigns these parameters for each scene to obtain diverse weather conditions, but the user has the option to set any of these parameters to a fixed value. For instance, setting the sun altitude angle to anything less than zero creates nighttime scenes.

Traffic. SimBEV randomly selects background vehicles from CARLA's vehicle library, which includes sedans, vans, trucks, heavy goods vehicles (HGVs), buses, bicycles, motorcycles, and emergency vehicles (firetruck, ambulance, and police car). Emergency lights are randomly turned on for the latter vehicles, and the user can set the probability that this happens (by default 0.5). When possible, vehicle colors are randomly selected from a set of recommended colors, so e.g. a sedan can have one of 160 standard colors, but the firetruck will always be red. Additionally, some CARLA vehicles support articulated doors, so when these vehicles come to a stop (e.g. at a traffic light), SimBEV may randomly open one or all of their doors.

SimBEV randomly selects each vehicle's maximum speed (relative to the speed limit, e.g. 10% over or under) and how close that vehicle can get to the vehicle in front of it when stopped. It also randomly selects how long each traffic light stays green. However, the user has the option to set any of these parameters to a fixed value.

SimBEV randomly selects pedestrians from CARLA's walker library (which contains models of different ages, genders, races, and body types), sets their walking speed at random, and gives them random destinations to go to.

Lights. SimBEV allows the user to turn off street and/or building lights (which are automatically turned on at night). Moreover, the user can choose to randomize building light colors, and/or change the intensity of all street lights by a fixed, if desired random, value. Moreover, based on the probability set by the user, SimBEV randomly turns off individual street lights to simulate broken street lights in the real world.



Figure 2. Reckless ego vehicle running over a cyclist.

Reckless driving and jaywalking. If desired by the user, some vehicles (including the ego vehicle) may drive recklessly, ignoring traffic lights, traffic signs, and collision with other vehicles and pedestrians, as shown in Fig. 2. The user can control the likelihood of reckless driving which can create interesting edge cases. Additionally, the user has control over the share of pedestrians who are allowed to (but may or may not) cross the road at any point, not just at crosswalks.

3.4. Data annotations

SimBEV currently offers two main annotation types: 3D object bounding boxes and BEV ground truth. The output of some perception sensors (e.g. segmentation, depth, and optical flow cameras) can be used as annotation as well, but they are not discussed here.

3D object bounding boxes. SimBEV currently collects 3D object bounding boxes that are within a user-configurable radius of the ego vehicle (by default 120.0 m) at each time step for the following six classes: car, truck (includes trucks, vans, HGVs, etc., but not buses), bus, motorcycle, bicycle, and pedestrian. SimBEV collects other object attributes alongside each bounding box such as the object’s ID, its linear and angular velocities, and its make, model, and color if the object is a vehicle. An optional post-processing step calculates the number of lidar and radar points that fall within each bounding box and adds a *valid* label to boxes with at least one point inside, *invalid* otherwise. This labeling is useful when training 3D object detection algorithms, as it can filter out objects that are not guaranteed to be visible by the perception sensors [2].

BEV segmentation. Getting accurate BEV ground truth is the most critical aspect of SimBEV, which currently supports the following eight classes: road, car, truck, bus, motorcycle, bicycle, rider (human on a motorcycle or bicycle), and pedestrian. At each time step, the BEV ground truth is saved as a $C \times l \times l$ binary array, where C is the number of



Figure 3. Ground elements in CARLA use one-way visible materials.

classes and l is the dimension of the BEV grid centered on the ego vehicle.

To calculate the BEV ground truth for non-road classes, we leverage the fact that ground elements in CARLA (roads, sidewalks, etc.) use one-way visible materials, i.e. they are see-through from the bottom, as shown in Fig. 3. This means that we can place a semantic segmentation camera 1 km above the ego vehicle facing down (to minimize perspective distortion) and another one 1 km below the ego vehicle facing up to catch what the overhead camera may miss because of obstructions. Both cameras have a $l \times l$ resolution and the FoV is calculated such that each pixel represents a $d \times d$ area on the ground. The ground truth for each non-road class is obtained by merging data from the two cameras using a *logical or* operation. By default, l is set to 360 and d is set to 0.4 m, creating a 144 m \times 144 m box around the ego vehicle. This is larger than what is typically used for BEV segmentation (100 m \times 100 m), but the additional area can help with data augmentation (rotation, translation, scaling) during training.

We follow an approach similar to [68] to get the ground truth for the road class. Specifically, we generate waypoints within a small distance of each other (specified by the user, we recommend setting it to d) across the map’s roads and note each waypoint’s lane width. We then calculate the mutual distance between these waypoints and the center of each cell of a $l \times l$ BEV grid centered on the ego vehicle where each cell represents a $d \times d$ area. For each grid cell, if a waypoint exists whose distance to the center of that cell is less than that waypoint’s lane width, that cell is labeled as road. Where our approach differs from [68] is that we then combine this information with data from the overhead camera and pass it through a *binary closing* operation to patch any potential holes, obtaining a more accurate ground truth.

Overall, this approach results in accurate BEV ground truth data and also lets us assign multiple labels to the same cell. For instance, a cell occupied by a rider on a motorcycle will have a rider label (obtained from the overhead camera), a motorcycle label (obtained from the underground camera), and a road label (obtained using the waypoints).

Map	Train	Validation	Test
Town01	8	2	2
Town02	8	2	2
Town03	20	4	4
Town04	20	4	4
Town05	20	4	4
Town06	20	4	4
Town07	20	4	4
Town10HD	20	4	4
Town12	48	8	8
Town13	0	8	8
Town15	36	6	6
Total	220	50	50

Table 2. Distribution of SimBEV dataset scenes across all available CARLA maps.

Our approach works everywhere except when roads with large elevation differences are present near the ego vehicle, e.g. when approaching an overpass. In those situations we do not use the semantic segmentation cameras. Instead, we only use the waypoint approach to calculate the road ground truth, and use 3D object bounding boxes to calculate the ground truth for other classes. While not as accurate as the previous method, the resulting ground truth is still acceptable. SimBEV intelligently switches between the two approaches when it detects two waypoints within 48.0 m of each other that have an elevation difference of at least 6.4 m, indicating they are on two different roads.

4. The SimBEV Dataset

To showcase SimBEV, we used it to generate the SimBEV dataset, a collection of 320 scenes spread across all 11 CARLA maps according to Tab. 2. Because Town12 and Town13 (CARLA’s two large maps) share many common features but use different building styles, textures, and vegetation, Town13 is not included in the train set to evaluate the generalization performance of trained perception models and expose overfitting issues.

To create the SimBEV dataset, we used every sensor supported by SimBEV (RGB, semantic segmentation, instance segmentation, depth, and optical flow cameras; regular and semantic lidar; radar; GNSS; and IMU), positioned on the ego vehicle (a 2016 Ford Mustang) as shown in Fig. 4. We used a time step of 50 ms (i.e. 20 FPS), with each scene lasting 16 s (320 frames). In total, the SimBEV dataset contains 102,400 annotated frames, 8,315,935 3D bounding boxes (3,792,499 of which are *valid*), and 2,793,491,357 BEV ground truth labels. With 81.2 3D bounding boxes per frame (37.0 *valid* boxes per frame) it is on par with, if not surpassing, existing driving datasets [2, 4, 54, 62, 63]. A collection of front camera images displayed in Fig. 5 highlights the diversity of the SimBEV dataset.

More information about the SimBEV dataset, including

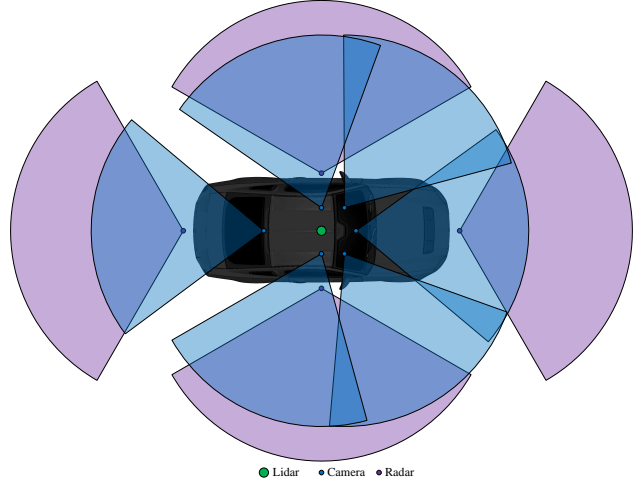


Figure 4. Position and FoV of the perception sensors used in SimBEV to create the SimBEV dataset.

sensor properties, SimBEV parameters, and dataset statistics can be found in the Supplementary Material.

5. Evaluation and Analysis

The SimBEV dataset supports a variety of tasks including 2D and 3D segmentation, depth and optical flow estimation, tracking, prediction, and localization. Here, however, we focus on the two most common tasks: BEV segmentation and 3D object detection.

5.1. Tasks and metrics

We use the intersection over union (IoU) metric for the BEV segmentation task, where for each class, a prediction is considered positive if its probability (score) is above a certain threshold. Although we calculate the IoU for each class for thresholds from 0.1 to 0.9 in increments of 0.1, we only report the values for a 0.5 threshold here. Complete results can be found in the Supplementary Material.

Our 3D object detection task metrics are inspired by [2], and rely on the Average Precision (AP) metric. We use two different methods to define a match between a predicted 3D bounding box and a ground truth one. In the first, two boxes are considered a match when their 3D IoU is above a certain threshold [6, 12]. In the second, two boxes are considered a match if the distance between their centers is below a certain threshold. As explained in [2], small translation errors for small objects (such as pedestrians) result in a low or even zero IoU value, which makes comparing the performance of camera-only models that tend to have large localization errors difficult.

For both approaches, the AP is calculated as the area under the precision-recall curve. For the first method, we use matching IoU thresholds of $\mathbb{T} =$

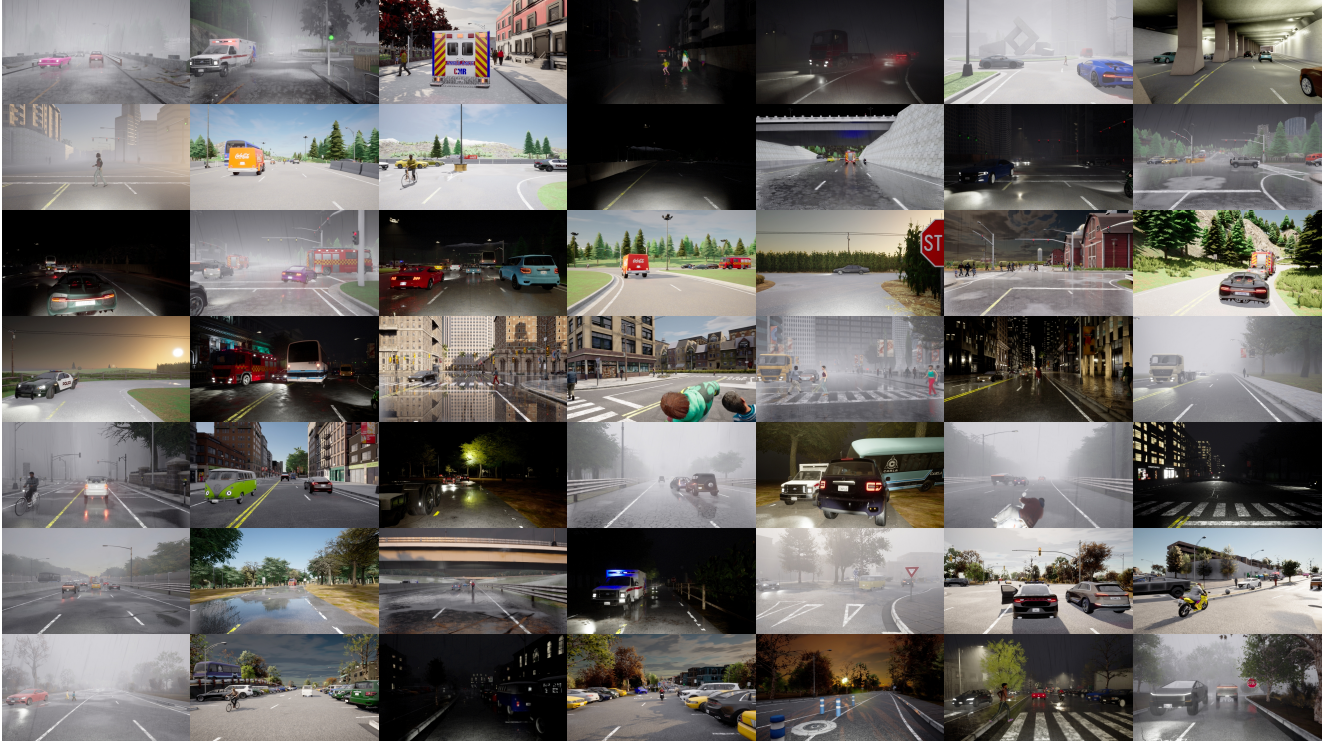


Figure 5. Front camera image samples from the SimBEV dataset.

$\{0.3, 0.4, 0.5, 0.6, 0.7, 0.8, 0.9\}$. For the second method, similar to [2], we use matching distance thresholds of $\mathbb{T} = \{0.5, 1, 2, 4\}$ m. For both approaches we define mAP as the average over all classes and all matching thresholds:

$$\text{mAP} = \frac{1}{|\mathbb{T}||\mathbb{C}|} \sum_{t \in \mathbb{T}, c \in \mathbb{C}} \text{AP}_{t,c}. \quad (1)$$

Similar to [2], we measure a set of True Positive metrics (TP metrics) for each predicted bounding box that is matched to a ground truth box. They are Average Translation Error (ATE), which is the Euclidean distance (in m) between box centers; Average Orientation Error (AOE), which is the smallest yaw angle difference (in rad) between the two boxes; Average Scale Error (ASE), which is equal to one minus the 3D IoU value of the two boxes after aligning for orientation and translation; and Average Velocity Error (AVE), which is the L2 norm of the difference in box velocities (in m/s). The mean TP metric (mTP) for each metric is computed by averaging over all classes and thresholds:

$$\text{mTP} = \frac{1}{|\mathbb{T}||\mathbb{C}|} \sum_{t \in \mathbb{T}, c \in \mathbb{C}} \text{TP}_{t,c}. \quad (2)$$

Finally, similar to [2], we define the SimBEV Detection Score (SDS) as:

$$\text{SDS} = \frac{1}{8} \left(4 \text{mAP} + \sum_{\text{mTP} \in \mathbb{TP}} (1 - \min(1, \text{mTP})) \right). \quad (3)$$

5.2. Evaluation results

We used BEVFusion [35], a state-of-the-art multi-sensor model for multi-task 3D perception, to evaluate both BEV segmentation and 3D object detection on the SimBEV dataset. BEVFusion offers camera-only, lidar-only, and fused (camera + lidar) model variants for each task (six variants in total), which lets us compare the performance of different sensing modalities. We trained all variants of BEVFusion using a batch size of 64, and sampled every 4th frame of the *train* set (17,600 samples in total). Furthermore, because of the imbalance in the number of objects for each class, we used the class-balanced grouping and sampling scheme utilized in the original implementation of BEVFusion [35, 76]. We used the *validation* set to tune a few hyperparameters, and evaluated the trained models on the *test* set. More information about BEVFusion and our training and evaluation strategy are provided in the Supplementary Material.

Tab. 3 shows BEV segmentation IoU values (in %) for the three BEVFusion variants. As expected, all models achieve higher IoU values for larger objects compared to smaller ones (*motorcycle, bicycle, rider, pedestrian*). Moreover, IoU values for the *road* class (which is the only BEV segmentation class shared between SimBEV and nuScenes) are consistent with [35].

We can see from Tab. 3 that the fused model performs

Modality	Road	Car	Truck	Bus	Motorcycle	Bicycle	Rider	Pedestrian	Mean
C	74.1	26.7	17.0	29.5	0.0	0.0	0.0	0.0	18.4
L	89.6	75.8	77.5	84.8	44.6	4.0	38.5	27.7	55.3
C + L	89.9	77.0	79.3	84.8	45.7	4.5	37.7	32.7	56.5

Table 3. BEV segmentation IoU values (in %) for different variants of BEVFusion evaluated on the SimBEV *test* set.

Modality	mAP (%) \uparrow	mATE (m) \downarrow	mAOE (rad) \downarrow	mASE \downarrow	mAVE (m/s) \downarrow	SDS (%) \uparrow
C	8.0	0.313	0.561	0.100	5.35	29.3
L	36.0	0.088	0.114	0.070	4.71	52.1
C + L	36.8	0.085	0.111	0.062	4.56	52.7

Table 4. 3D object detection results for different variants of BEVFusion evaluated on the SimBEV *test* set using the first method.

Modality	mAP (%) \uparrow	mATE (m) \downarrow	mAOE (rad) \downarrow	mASE \downarrow	mAVE (m/s) \downarrow	SDS (%) \uparrow
C	22.7	0.708	0.686	0.131	4.92	29.8
L	46.2	0.151	0.201	0.109	4.62	54.9
C + L	46.3	0.148	0.198	0.097	4.48	55.1

Table 5. 3D object detection results for different variants of BEVFusion evaluated on the SimBEV *test* set using the second method.

the best, followed closely by the lidar-only model because our lidar point cloud is very dense (approximately 225,000 points per frame). The fused model sees a 5% improvement in *pedestrian* IoU values, where it is helped by the additional semantic information from the camera. However, both models perform poorly when it comes to the *bicycle* class, though we found that the fused model achieves an IoU value of 17.9% for the *bicycle* class when the threshold is lowered to 0.4. It seems that because bicycles are always accompanied by a rider (and smaller and less noticeable than motorcycles), the model has difficulty distinguishing between the two and has lower confidence in its predictions.

Tab. 3 also shows that the camera-only model performs poorly (except for the *road* class) compared to the other two, and reports a 0 IoU value for the smaller classes. As noted before, because images lack explicit geometric information, camera-only models have difficulty localizing objects.

3D object detection results using the first and second methods are shown in Tab. 4 and Tab. 5, respectively, and a comprehensive breakdown of the results is provided in the Supplementary Material. Like before, the fused model performs the best, followed closely by the lidar-only model. We can see that the second method produces higher mAP values, which is due to its more permissive nature where, unlike the first method, two boxes can be matched even if they do not intersect at all. This permissiveness, which makes the camera-only model more comparable to the other two, can be seen when juxtaposing the mATE, mAOE, and mASE values of the two methods, with those for the second method being considerably higher. Interestingly enough, this seems to indicate that both methods result in similar SDSs. As for the large mAVE values, because none of the input data has any embedded velocity information, it is hard for the model to estimate an object’s velocity. As noted in [2], aggregating consecutive point clouds decorated by their timestamp can significantly improve mAVE.

Finally, we should note that the Swin-T [34] model used as BEVFusion’s image encoder was pretrained on ImageNet [8] and nuImages [2], which means the performance of models with image input may be less than optimal due to domain shift. Pretraining Swin-T using CARLA-based data may improve performance.

6. Conclusion

In this paper we introduce SimBEV, an extensively configurable and scalable randomized synthetic data generation tool that collects accurate BEV ground truth data and supports a variety of configurable perception and localization sensors. We hope that SimBEV enables users to rapidly create and scale different driving datasets, making it an invaluable tool for empowering researchers to explore various computer vision tasks. To showcase SimBEV, we use it to create the SimBEV dataset, a comprehensive large-scale driving dataset, which we use to benchmark BEV perception models and compare different sensing modalities and evaluation approaches. Future work will focus on expanding object classes supported by SimBEV, supporting custom sensor positions, and enabling V2X data collection.

SimBEV: A Synthetic Multi-Task Multi-Sensor Driving Data Generation Tool and Dataset

Supplementary Material

A. CARLA Simulator

SimBEV relies on a modified version of CARLA Simulator 0.9.15 [9] with an enhanced content library. Some of the improvements we made are listed below.

- We added three new sports cars to CARLA’s vehicle library using existing 3D models [22]¹: sixth generation Ford Mustang, Toyota GR Supra, and Bugatti Chiron, shown in Fig. 6. They increase the diversity of CARLA’s vehicle library, especially when it comes to fast, high-performance vehicles. The Ford Mustang is the default vehicle for collecting SimBEV data.
- We added lights (headlights, taillights, blinkers, etc.) to some of the older vehicle models in CARLA’s library lacking them, and redesigned existing vehicle lights in Blender using a new multi-layer approach that better visualizes modern multi-purpose lights, as shown in Fig. 7.
- We added a set of 160 standard colors for most vehicle models to choose from (apart from a few like the firetruck), and fixed color randomization issues for a few vehicles (e.g. the bus).
- We updated the vehicle dynamics parameters of vehicle models to better match their vehicle’s behavior and performance in the real world.
- We added or updated pedestrian navigation information for CARLA’s Town12, Town13, and Town15 maps.
- We updated the motorcycle and bicycle models so they select their driver models randomly each time, instead of always being assigned the same model.
- We added lights to buildings in Town12 and fixed issues that prevented full control over building/street lights in Town12 and Town15.

SimBEV is compatible with the standard version of CARLA 0.9.15, but some features may not work properly.

B. The SimBEV Dataset

B.1. SimBEV configuration

We configured SimBEV toward generating diverse scenarios when creating the SimBEV dataset, and collected data from every sensor supported by SimBEV (RGB, semantic segmentation, instance segmentation, depth, and optical flow cameras; regular and semantic lidar; radar; GNSS; and IMU). The configuration used for each sensor type is listed

¹We used royalty-free 3D models of the three cars available on BlenderKit as the basis for the vehicles. However, the Supra and Chiron models had been removed from BlenderKit at the time of writing, so unfortunately we have no way of crediting their authors for their work.



Figure 6. From left to right, the Bugatti Chiron, Ford Mustang, and Toyota GR Supra vehicles added to CARLA’s vehicle library with their lights turned off (top) and on (bottom).



Figure 7. In contrast to CARLA’s segmented light design approach, our multi-layer approach can realistically visualize vehicle lights that use the same element for multiple purposes. For instance, in the Ford Mustang pictured here both position and left blinker lights are turned on.

in Tab. 6 and the arrangement of sensors on the ego vehicle is detailed in Tab. 7.

Our sensor setup was mostly inspired by [2] (e.g. the 1600×900 image resolution, the arrangement of the cameras, and the lidar’s vertical FoV), though there are a few differences. Our lidars (regular and semantic) have 128 channels instead of 32 to collect a much denser point cloud, which can be downsampled by the user later on if desired.

Sensor type	Properties
RGB camera	1600×900 resolution, 80 deg FoV, $f/1.8$
All other cameras	1600×900 resolution, 80 deg FoV
Lidar	128 channels, 120.0 m range, 20.0 Hz rotation frequency, 5,242,880 points per second, 10.67 to -30.67 vertical FoV, 14% general drop-off rate, 1 cm radial noise std
Semantic lidar	128 channels, 120.0 m range, 20.0 Hz rotation frequency, 5,242,880 points per second, 10.67 to -30.67 vertical FoV
Radar	120.0 m range, 100 deg horizontal FoV, 12 deg vertical FoV, 40,000 points per second
GNSS	{4e-2 m, 4e-7 deg, 4e-7 deg} noise std for {altitude, latitude, longitude}
IMU	1.7e-4 rad/s gyroscope bias, {1.7e-4 m/s ² , 5.6e-6 rad/s} noise std for {accelerometer, gyroscope}

Table 6. Sensor configurations used for the collection of the SimBEV dataset. std: standard deviation.

Sensor	x (m)	y (m)	z (m)	γ (deg)
Front left camera	0.4	0.4	1.6	55
Front camera	0.6	0.0	1.6	0
Front right camera	0.4	-0.4	1.6	-55
Back left camera	0.0	0.4	1.6	110
Back camera	-1.0	0.0	1.6	180
Back right camera	0.0	-0.4	1.6	-110
Left radar	0.0	1.0	0.6	90
Front radar	2.4	0.0	0.6	0
Right radar	0.0	-1.0	0.6	-90
Back radar	-2.4	0.0	0.6	180
Lidar	0.0	0.0	1.8	N/A

Table 7. Arrangement of data collection sensors used in SimBEV and the SimBEV dataset. Coordinates are relative to the center of the ground plane of the ego vehicle’s 3D bounding box.

For the GNSS and IMU we used bias and noise standard deviation values of a GNSS/INS module found in a typical experimental autonomous driving platform.

SimBEV uses the probability distributions listed in Tab. 8 to randomize the parameters that control weather in CARLA. These distributions are interdependent to ensure the resulting weather is realistic (e.g. a combination of heavy rain and clear sky is unrealistic). Each of the configured parameters is briefly discussed below.

- Cloudiness controls the amount of clouds. Values range from 0 to 100, 0 being a clear sky.
- Precipitation controls the intensity of rain. Values range from 0 to 100, 0 being no rain.
- Precipitation deposits controls the amount of puddles. Values range from 0 to 100, 0 being no puddles and 100 a road filled with water.
- Wetness controls camera image blurriness caused by rain. Values range from 0 to 100, 0 being no blurriness.
- Wind intensity controls the strength of wind. Values range from 0 to 100, 0 being no wind at all.
- Sun azimuth angle controls the azimuth angle of the sun. Values range from 0 to 360.
- Sun altitude angle controls the altitude angle of the sun. Values range from -90 to 90, -90 being midnight and 90 being midday.
- Fog density controls fog concentration or thickness. Val-

Parameter	Symbol	Distribution
Cloudiness	k_c	$100 \times \mathcal{B}(0.8, 1.0)$
Precipitation	k_p	$\mathcal{B}(0.8, 0.2) \times k_c$ if $k_c > 40.0$ else 0.0
Precipitation deposits	k_{pd}	$k_p + \mathcal{B}(1.2, 1.6) \times (100 - k_p)$
Wetness	k_w	$\min(100.0, \max(\mathcal{N}(k_p, 10.0)))$
Wind intensity	k_{wi}	$\mathcal{U}(0.0, 100.0)$
Sun azimuth angle	k_{az}	$\mathcal{U}(0.0, 360.0)$
Sun altitude angle	k_{al}	$180 \times \mathcal{B}(3.6, 2.0) - 90.0$
Fog density	k_f	$100 \times \mathcal{B}(1.6, 2.0)$ if $k_c > 40.0$ or $k_{al} < 10.0$ else 0.0
Fog distance	k_{fd}	$\mathcal{LN}(3.2, 0.8)$ if $k_f > 10.0$ else 0.0
Fog falloff	k_{ff}	$5.0 \times \mathcal{B}(1.2, 2.4)$ if $k_f > 10.0$ else 1.0

Table 8. Probability distribution of SimBEV weather parameters. \mathcal{B} : beta distribution. \mathcal{N} : normal distribution. \mathcal{U} : uniform distribution. \mathcal{LN} : log-normal distribution.

ues range from 0 to 100, 0 being no fog.

- Fog distance controls how far away the fog starts. Values can be any nonnegative number.
- Fog falloff controls the density of the fog (as in specific mass). Values can be any nonnegative number. If set to 0, the fog will be lighter than air and will cover the whole scene. If set to 1, the fog is approximately as dense as air. For values greater than 5 the fog will be so dense that it will be compressed to the ground level. Fog falloff is set to 0.01 in Town12, Town13, and Town15 due to their non-zero elevation.

SimBEV leaves other weather parameters (such as scattering intensity and dust storm) at their default value, though the user can change them if desired.

Table 9 lists several other SimBEV configurations used to create the SimBEV dataset. They control various aspects of SimBEV such as scene duration, number of spawned background vehicles and pedestrians, driving behavior, chance of reckless driving, etc.

B.2. SimBEV dataset statistics

The SimBEV dataset comprises 102,400 annotated frames, 8,315,935 3D bounding boxes (3,792,499 of which are

Parameter	Value or distribution
Warmup duration	4 s
Scene duration	16 s
Simulation time step	50 ms
3D bounding box collection radius	120.0 m
BEV grid resolution	360×360
BEV grid cell dimensions	$0.4 \text{ m} \times 0.4 \text{ m}$
Distance between generated waypoints used for BEV ground truth calculation	0.4 m
Distance between generated waypoints used as spawning points	24.0 m
Number of spawned background vehicles (s : number of available spawn points)	$\mathcal{U}_i(0, s - 3)$
Number of spawned pedestrians	$\mathcal{U}_i(0, 640)$
Radius around the ego vehicle where background vehicles and pedestrians are spawned	400.0 m
Probability of vehicles opening door(s) when stopped	10.0%
Probability of emergency lights turned on	50.0%
Probability of ego vehicle being reckless	1.0%
Probability of other vehicles being reckless	1.0%
Minimum pedestrian speed	0.8 m/s
Maximum pedestrian speed (r : minimum pedestrian speed)	$\max(r, \mathcal{LN}(0.16, 0.64)) \text{ m/s}$
Minimum street light intensity	10,000 lm
Change in street light intensity (m : average street light intensity of the scene)	$\mathcal{U}(-m, m) \text{ lm}$
Probability of street light failure	10.0%
Maximum vehicle speed relative to the speed limit	$\mathcal{U}(-20.0, 40.0)\%$
Distance to front vehicle when stopped	$\mathcal{N}(3.2, 1.0) \text{ m}$
Traffic light green time	$\mathcal{U}(4.0, 28.0) \text{ s}$
Walker cross factor	$\mathcal{B}(2.4, 1.6)$

Table 9. SimBEV configuration used for the collection of the SimBEV dataset. \mathcal{B} : beta distribution. \mathcal{N} : normal distribution. \mathcal{U} : uniform distribution. \mathcal{U}_i : uniform integer distribution. \mathcal{LN} : log-normal distribution.

Class	Total 3D bounding boxes	Valid 3D bounding boxes	BEV labels
Road	N/A	N/A	2,674,391,899
Car	2,935,809	1,495,066	84,073,215
Truck	497,729	298,280	22,759,787
Bus	67,880	46,754	7,546,007
Motorcycle	297,132	146,083	858,136
Bicycle	214,619	100,640	187,869
Rider	N/A	N/A	510,521
Pedestrian	4,302,766	1,705,676	3,163,923
Total	8,315,935	3,792,499	2,793,491,357

Table 10. Breakdown of total and *valid* 3D bounding boxes and BEV ground truth labels by class for the SimBEV dataset.

valid), and 2,793,491,357 BEV ground truth labels, broken down by class in Tab. 10. Cars and pedestrians make up the largest share of 3D bounding boxes, though they include a large number of motorcycles and bicycles as well. This makes sense given that the majority of models in CARLA’s vehicle library are cars (as opposed to e.g. only one bus model). BEV labels are dominated by the road class, followed by cars, trucks, and buses due to their larger footprint compared to the rest.

As discussed previously, SimBEV randomizes CARLA’s weather parameters according to the distributions specified in Tab. 8. Figure 8 shows the distribution of weather across the SimBEV dataset, where precipitation (rain intensity, k_p) and fog density (k_f) values for each scene are categorized

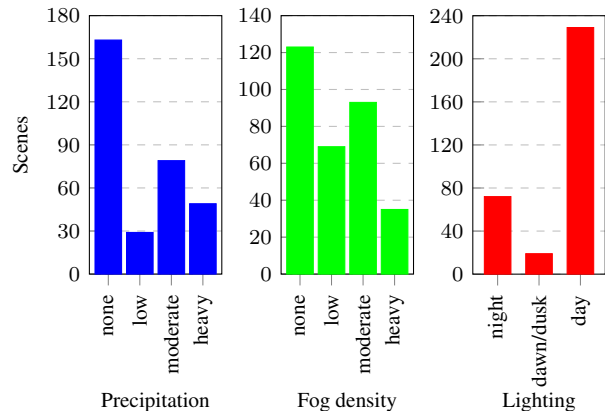


Figure 8. Distribution of weather across SimBEV dataset scenes.

into none (<10%), low (10 - 40%), moderate (40 - 70%), and heavy (70 - 100%); while sun altitude angle (k_{at}) is categorized into night (-90 - 0 deg), dawn/dusk (0 - 6 deg), and day (6 - 90 deg). Figure 8 shows that SimBEV contains a good mix of different weather conditions, with either rain or fog present in around half of the scenes and nearly a quarter of the scenes occurring at night.

Looking at the distribution of the number of spawned vehicles (includes cars, trucks, buses, motorcycles, bicycles) and pedestrians among SimBEV dataset scenes shown in Fig. 9, it is clear that the scenes range from relatively empty to congested and crowded. The distribution of pedestrians

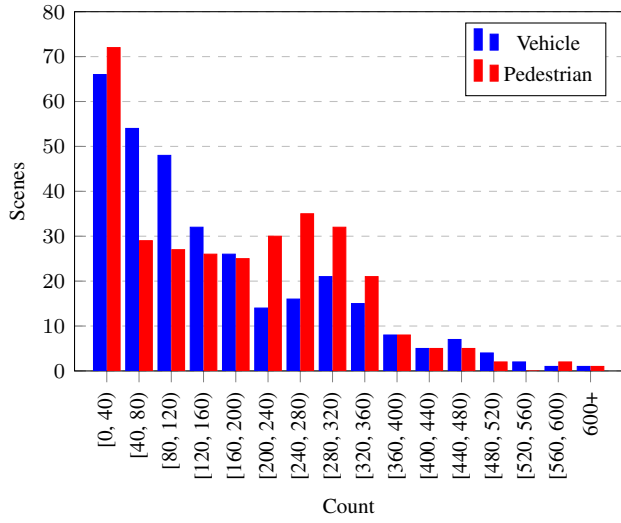


Figure 9. Distribution of the number of spawned vehicles (includes cars, trucks, buses, motorcycles, and bicycles) and pedestrians across SimBEV dataset scenes.

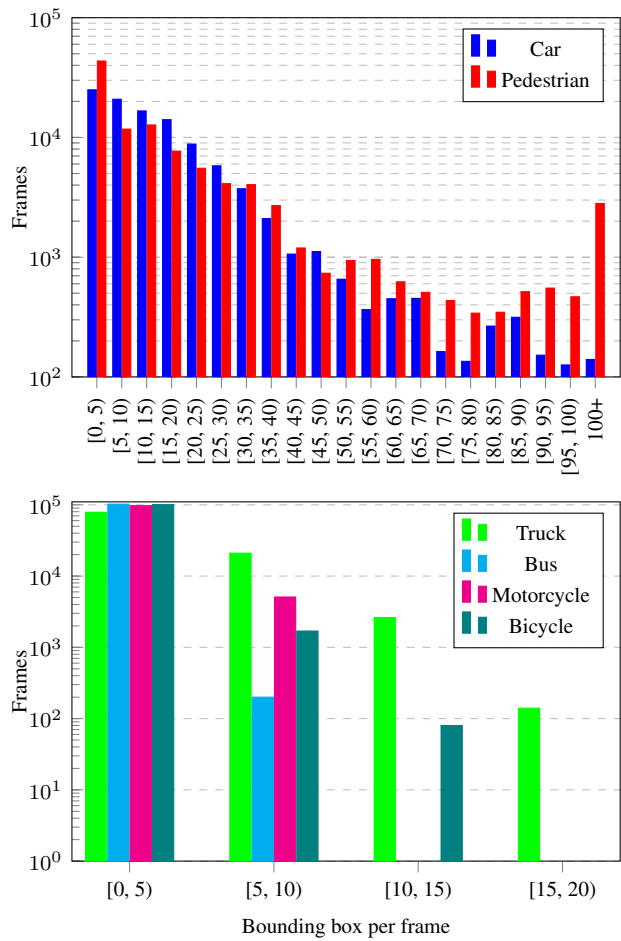


Figure 10. Breakdown of the number of valid 3D object bounding boxes per frame by class across the SimBEV dataset.

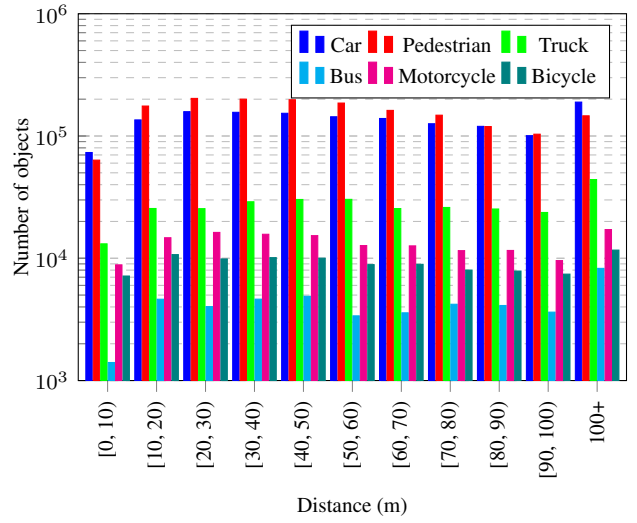


Figure 11. Distribution of the distance of valid objects from the ego vehicle across the SimBEV dataset.

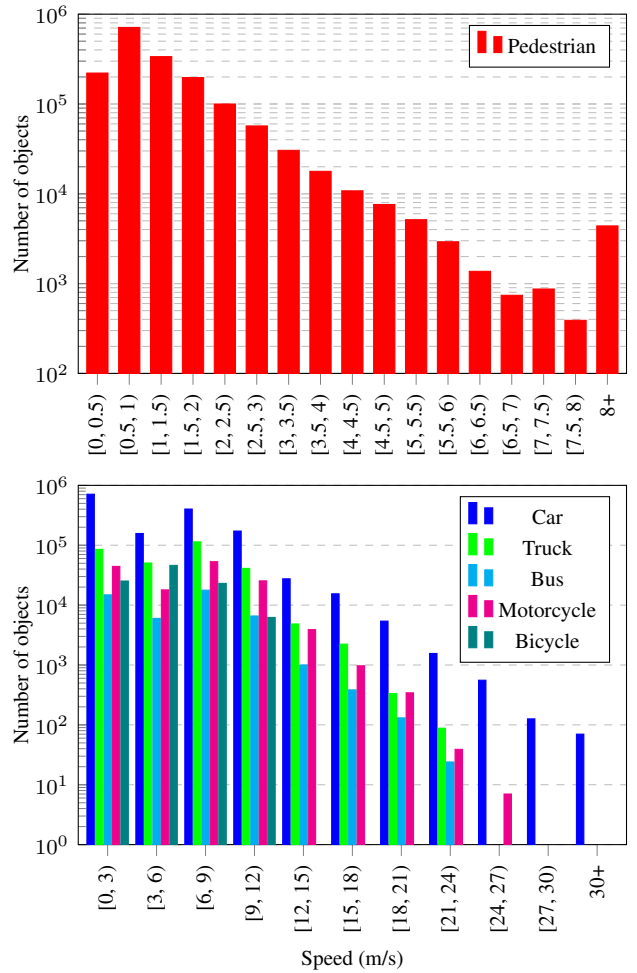


Figure 12. Breakdown of the speed of valid objects across the SimBEV dataset.

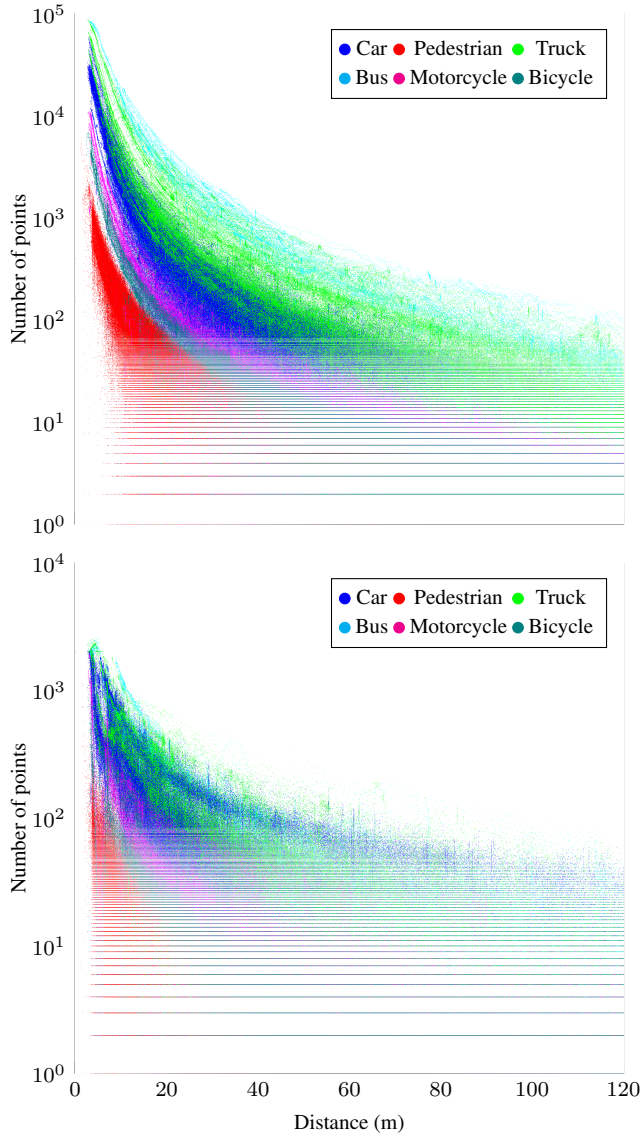


Figure 13. Distribution of the number of lidar (top) and radar (bottom) points within *valid* 3D object bounding boxes with respect to distance from the ego vehicle.

is supposed to be uniform, but CARLA often spawns fewer pedestrians than requested, and the number of unspawned pedestrians grows rapidly when hundreds of pedestrians are requested. Hence there are many scenes with 240 - 320 pedestrians and very few with more than 480.

Because Fig. 9 shows the total number of spawned vehicles and pedestrians, many of which may be far from the ego vehicle, it does not paint the full picture of what the ego vehicle observes. Hence in Fig. 10 we break down the number of *valid* 3D object bounding boxes per frame by class for the SimBEV dataset. The distribution of the bounding boxes is similar to [2], though our dataset offers a sizable number of frames with many (65+) *valid* car or pedestrian

bounding boxes as well. As expected, due to fewer models in CARLA’s vehicle library, the vast majority of frames only include a handful of trucks, buses, motorcycles, and bicycles.

For more insight into the SimBEV dataset we turn to Fig. 11 through Fig. 13. Figure 11 shows that 3D object bounding box distances from the ego vehicle are nearly uniformly distributed for all classes, in contrast to [2], which is likely due to the higher density and range of our lidar point cloud. Figure 12 shows a reasonable speed range for all object classes, which is comparable to [2] with a few exceptions. We have a large number of running pedestrians (3+ m/s) which can act as edge cases for perception and behavior prediction algorithms. For other classes, our data is collected from both urban and highway environments (unlike [2] which only collected data from urban environments), leading to many fast-moving objects. Figure 13 shows the distribution of the number of lidar and radar points within *valid* 3D object bounding boxes with respect to distance. Consistent with [2], larger object bounding boxes have more points inside and the number of points for all classes decrease with increasing distance.

Finally, logarithmic BEV ground truth label heat maps of the SimBEV dataset for all classes are shown in Fig. 14. As expected, there is a concentration of road labels in the ego vehicle’s direction of travel, which also results in a concentration of labels in that region for all vehicular classes. In contrast, pedestrian labels are relatively evenly distributed.

C. BEVFusion Implementation Details

All variants of BEVFusion [35] were trained on an Nvidia DGX A100 640GB node using sigmoid focal loss [29] and a batch size of 64. We used the original BEVFusion implementation’s settings to train the 3D object detection models, i.e. we employed the AdamW optimizer [38] with a weight decay factor of 0.01. The camera-only, lidar-only, and fused models used an initial learning rate of $2e-4$, $1e-4$, and $2e-4$, respectively. A cyclic learning rate scheduler [52] was used for the first two models, and cosine annealing [37] was used for the latter. All three models were trained for 20 epochs. BEVFusion’s BEV segmentation variants were trained for 40 epochs using an initial learning rate of $3e-5$ and a cyclic learning rate scheduler with a 4.0 target ratio. Input data was augmented (translated, rotated, scaled) for the training of all BEVFusion variants.

D. Comprehensive Evaluation Results

BEV segmentation IoU values (in %) by class and IoU threshold for the three BEVFusion variants are shown in Tab. 11, and 3D object detection AP values (in %) by class and threshold are shown in Tab. 12 and Tab. 13 for the first and second methods, respectively. As discussed before, the

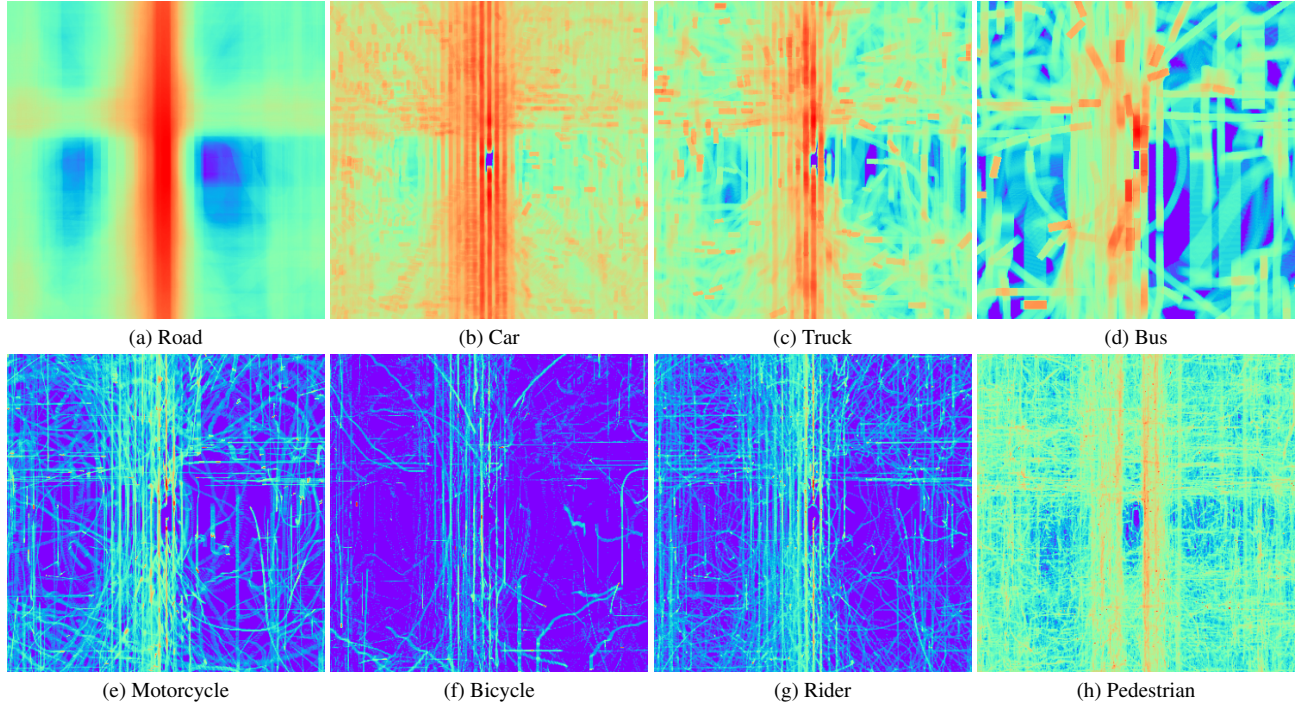


Figure 14. Logarithmic BEV heat map of the SimBEV dataset for different classes.

Class	0.1	0.2	0.3	0.4	0.5	0.6	0.7	0.8	0.9
Road	64.1	69.1	71.6	73.3	74.1	73.8	72.6	70.5	66.4
Car	6.3	12.7	22.7	28.4	26.7	19.5	15.2	11.6	9.5
Truck	5.7	13.7	18.8	19.7	17.0	12.3	7.2	2.9	0.3
Bus	11.4	23.1	29.1	30.8	29.5	25.6	19.4	11.8	4.5
Motorcycle	0.4	2.5	1.2	0.2	0.0	0.0	0.0	0.0	0.0
Bicycle	0.1	0.0	0.0	0.0	0.0	0.0	0.0	0.0	0.0
Rider	0.3	1.0	0.2	0.1	0.0	0.0	0.0	0.0	0.0
Pedestrian	0.2	0.0	0.0	0.0	0.0	0.0	0.0	0.0	0.0
Mean	11.0	15.3	18.0	19.1	18.4	16.4	14.3	12.1	10.1
Road	52.9	58.6	68.7	87.5	89.6	89.3	87.6	84.6	79.7
Car	6.5	41.0	60.8	72.2	75.8	68.6	57.2	45.0	28.8
Truck	14.7	49.1	66.0	75.1	77.5	71.1	60.2	47.5	29.2
Bus	27.0	65.6	78.8	84.2	84.8	79.5	70.6	60.3	46.2
Motorcycle	6.0	17.4	27.9	38.6	44.6	33.9	9.1	0.3	0.0
Bicycle	2.9	7.8	13.4	12.7	4.0	0.1	0.0	0.0	0.0
Rider	5.2	14.4	24.0	36.2	38.5	13.4	0.3	0.0	0.0
Pedestrian	3.0	11.0	19.7	31.4	27.7	2.1	0.0	0.0	0.0
Mean	14.8	33.1	44.9	54.7	55.3	44.8	35.6	29.7	23.0
Road	75.9	82.9	86.7	89.0	89.9	89.4	87.8	85.2	81.1
Car	20.3	46.1	63.8	73.8	77.0	70.0	59.2	47.5	32.3
Truck	26.1	53.8	66.7	75.5	79.3	73.8	63.2	51.3	33.8
Bus	39.6	69.0	79.9	84.5	84.8	80.3	72.5	63.1	49.7
Motorcycle	5.8	18.8	29.6	39.7	45.7	34.8	9.4	0.1	0.0
Bicycle	3.3	8.7	14.6	17.9	4.5	0.1	0.0	0.0	0.0
Rider	5.4	15.2	24.6	36.2	37.7	15.4	0.9	0.0	0.0
Pedestrian	2.8	11.3	19.9	31.6	32.7	5.8	0.1	0.0	0.0
Mean	22.4	38.2	48.2	56.0	56.5	46.2	36.6	30.9	24.6

Table 11. BEV segmentation IoU values (in %) by class and IoU threshold for the camera-only variant (top), lidar-only variant (middle), and fused variant (bottom) of BEVFusion.

Class	0.1	0.2	0.3	0.4	0.5	0.6	0.7	0.8	0.9
Car	33.0	29.4	23.8	17.8	12.3	7.1	2.0	0.2	0.0
Truck	30.3	27.0	23.0	18.5	13.8	9.7	5.1	1.5	0.0
Bus	31.5	30.3	27.5	25.1	21.5	15.5	10.0	5.7	0.0
Motorcycle	28.5	25.7	22.0	17.0	11.7	6.4	1.0	0.1	0.0
Bicycle	23.2	19.7	16.6	11.6	6.5	2.6	0.2	0.0	0.0
Pedestrian	2.2	1.0	0.5	0.2	0.1	0.0	0.0	0.0	0.0
Mean	24.8	22.2	18.9	15.0	11.0	6.9	3.1	1.3	0.0
Car	51.4	51.2	50.7	50.3	49.7	48.7	46.1	36.1	5.1
Truck	46.0	45.9	45.7	45.6	45.3	44.7	42.6	30.9	7.3
Bus	35.6	35.4	35.4	35.2	35.0	34.4	34.3	32.1	6.7
Motorcycle	48.1	47.3	46.6	46.0	45.3	44.3	41.5	26.3	1.4
Bicycle	56.5	56.5	56.2	55.8	55.1	52.2	42.3	23.9	0.9
Pedestrian	57.4	56.5	54.8	51.9	46.5	36.7	19.6	3.9	0.1
Mean	49.2	48.8	48.2	47.4	46.1	43.5	37.7	25.5	3.6
Car	51.5	51.3	50.8	50.4	49.8	48.9	46.5	37.2	7.2
Truck	46.2	46.0	45.8	45.7	45.3	44.7	43.4	34.0	11.4
Bus	35.6	35.6	35.5	35.4	35.2	34.9	34.3	32.1	11.8
Motorcycle	48.5	47.9	47.2	46.5	45.8	44.9	42.6	30.3	2.3
Bicycle	56.4	56.3	56.1	55.7	54.9	52.3	43.4	27.1	1.6
Pedestrian	57.3	56.6	54.7	52.0	46.7	37.7	20.8	4.5	0.1
Mean	49.2	48.9	48.4	47.6	46.3	43.9	38.5	27.5	5.7

Table 12. 3D object detection AP values (in %) by class and IoU threshold for the first method (3D IoU-based) for the camera-only variant (top), lidar-only variant (middle), and fused variant (bottom) of BEVFusion.

biggest takeaway from the results is that the camera-only variants (for both BEV segmentation and 3D object detec-

Class	0.5	1.0	2.0	4.0
Car	10.5	20.3	30.5	37.3
Truck	8.4	15.4	25.4	33.7
Bus	7.0	15.8	24.3	31.6
Motorcycle	16.5	26.4	31.9	34.7
Bicycle	15.6	22.1	27.7	29.7
Pedestrian	4.7	14.2	26.4	35.3
Mean	10.5	19.1	27.7	33.7
Car	34.9	45.0	51.2	51.8
Truck	21.8	36.2	45.9	46.4
Bus	34.3	34.8	35.4	35.6
Motorcycle	48.2	49.5	50.6	50.9
Bicycle	56.4	56.5	56.5	56.6
Pedestrian	38.1	52.8	59.8	60.7
Mean	38.9	45.8	49.9	50.3
Car	34.7	44.9	51.2	51.8
Truck	23.2	36.6	46.3	46.8
Bus	34.0	35.0	35.6	35.6
Motorcycle	48.0	49.1	50.2	50.8
Bicycle	56.3	56.4	56.4	56.4
Pedestrian	38.5	53.0	59.9	60.9
Mean	39.1	45.8	49.9	50.4

Table 13. 3D object detection AP values (in %) by class and distance threshold for the second method (distance-based) for the camera-only variant (top), lidar-only variant (middle), and fused variant (bottom) of BEVFusion.

tion) perform worse than the lidar-only and fused variants. Another takeaway is that compared to the first method, the second method for evaluating 3D object detection results allows for better comparison of the camera-only model results to that of the other two models, especially when it comes to smaller objects.

References

- [1] Mario Bijelic, Tobias Gruber, Fahim Mannan, Florian Kraus, Werner Ritter, Klaus Dietmayer, and Felix Heide. Seeing through fog without seeing fog: Deep multimodal sensor fusion in unseen adverse weather. In *CVPR*, pages 11682–11692, 2020. 1
- [2] Holger Caesar, Varun Bankiti, Alex H Lang, Sourabh Vora, Venice Erin Liong, Qiang Xu, Anush Krishnan, Yu Pan, Giancarlo Baldan, and Oscar Beijbom. nuScenes: A multimodal dataset for autonomous driving. In *CVPR*, pages 11621–11631. IEEE, 2020. 1, 3, 4, 5, 6, 7, 8
- [3] Hongxiang Cai, Zeyuan Zhang, Zhenyu Zhou, Ziyin Li, Wenbo Ding, and Jiuhua Zhao. BEVFusion4D: Learning lidar-camera fusion under bird’s-eye view via cross-modality guidance and temporal aggregation. *arXiv preprint arXiv:2303.17099*, 2023. 1
- [4] Ming-Fang Chang, John Lambert, Patsorn Sangkloy, Jagjeet Singh, Slawomir Bak, Andrew Hartnett, De Wang, Peter Carr, Simon Lucey, Deva Ramanan, et al. Argoverse: 3D tracking and forecasting with rich maps. In *CVPR*, pages 8748–8757, 2019. 3, 6
- [5] Kashyap Chitta, Aditya Prakash, Bernhard Jaeger, Zehao Yu, Katrin Renz, and Andreas Geiger. TransFuser: Imitation with transformer-based sensor fusion for autonomous driving. *IEEE TPAMI*, 45(11):12878–12895, 2023. 1
- [6] Marius Cordts, Mohamed Omran, Sebastian Ramos, Timo Rehfeld, Markus Enzweiler, Rodrigo Benenson, Uwe Franke, Stefan Roth, and Bernt Schiele. The CityScapes dataset for semantic urban scene understanding. In *CVPR*, pages 3213–3223, 2016. 3, 6
- [7] Can Cui, Yunsheng Ma, Xu Cao, Wenqian Ye, Yang Zhou, Kaizhao Liang, Jintai Chen, Juanwu Lu, Zichong Yang, Kuei-Da Liao, et al. A survey on multimodal large language models for autonomous driving. In *Proceedings of the IEEE/CVF Winter Conference on Applications of Computer Vision*, pages 958–979, 2024. 1
- [8] Jia Deng, Wei Dong, Richard Socher, Li-Jia Li, Kai Li, and Li Fei-Fei. ImageNet: A large-scale hierarchical image database. In *CVPR*, pages 248–255, 2009. 8
- [9] Alexey Dosovitskiy, German Ros, Felipe Codevilla, Antonio Lopez, and Vladlen Koltun. CARLA: An open urban driving simulator. In *Proceedings of the Conference on Robot Learning*, pages 1–16. PMLR, 2017. 3, 1
- [10] Prमित Dutta, Ganesh Sistu, Senthil Yogamani, Edgar Galván, and John McDonald. ViT-BEVSeg: A hierarchical transformer network for monocular bird’s-eye view segmentation. In *Proceedings of the 2022 International Joint Conference on Neural Networks (IJCNN)*, pages 1–7. IEEE, 2022. 1
- [11] Azim Eskandarian, Chaoxian Wu, and Chuanyang Sun. Research advances and challenges of autonomous and connected ground vehicles. *IEEE Transactions on Intelligent Transportation Systems*, 22(2):683–711, 2019. 1
- [12] Andreas Geiger, Philip Lenz, Christoph Stiller, and Raquel Urtasun. Vision meets robotics: The KITTI dataset. *The International Journal of Robotics Research*, 32(11):1231–1237, 2013. 3, 6
- [13] Shi Gong, Xiaoqing Ye, Xiao Tan, Jingdong Wang, Errui Ding, Yu Zhou, and Xiang Bai. GitNet: Geometric prior-based transformation for bird’s-eye view segmentation. In *ECCV*, pages 396–411. Springer, 2022. 1
- [14] James Gunn, Zygmunt Lenyk, Anuj Sharma, Andrea Donati, Alexandru Buburuzan, John Redford, and Romain Mueller. Lift-Attend-Splat: Bird’s-eye view camera-lidar fusion using transformers. In *CVPR*, pages 4526–4536, 2024. 1
- [15] Junyao Guo, Unmesh Kurup, and Mohak Shah. Is it safe to drive? An overview of factors, metrics, and datasets for driveability assessment in autonomous driving. *IEEE Transactions on Intelligent Transportation Systems*, 21(8):3135–3151, 2019. 1
- [16] John Houston, Guido Zuidhof, Luca Bergamini, Yawei Ye, Long Chen, Ashesh Jain, Sammy Omari, Vladimir Igloukov, and Peter Ondruska. One thousand and one hours: Self-driving motion prediction dataset. In *Conference on Robot Learning*, pages 409–418. PMLR, 2021. 1, 3
- [17] Junjie Huang, Guan Huang, Zheng Zhu, Yun Ye, and Dalong Du. BEVDet: High-performance multi-camera 3D object detection in bird’s-eye view. *arXiv preprint arXiv:2112.11790*, 2021. 1
- [18] Xinyu Huang, Xinjing Cheng, Qichuan Geng, Binbin Cao, Dingfu Zhou, Peng Wang, Yuanqing Lin, and Ruigang Yang. The ApolloScape dataset for autonomous driving. In *CVPRW*, pages 954–960, 2018. 3
- [19] Zhiyu Huang, Chen Lv, Yang Xing, and Jingda Wu. Multi-modal sensor fusion-based deep neural network for end-to-end autonomous driving with scene understanding. *IEEE Sensors Journal*, 21(10):11781–11790, 2020. 1
- [20] Zhijian Huang, Sihao Lin, Guiyu Liu, Mukun Luo, Chaoqiang Ye, Hang Xu, Xiaojun Chang, and Xiaodan Liang. Fuller: Unified multi-modality multi-task 3D perception via multi-level gradient calibration. In *ICCV*, pages 3502–3511, 2023. 1
- [21] Yang Jiao, Zequn Jie, Shaoxiang Chen, Jingjing Chen, Lin Ma, and Yu-Gang Jiang. MSMD Fusion: Fusing lidar and camera at multiple scales with multi-depth seeds for 3D object detection. In *CVPR*, pages 21643–21652, 2023. 1
- [22] Kentik khudosovtsev. Ford Mustang, 2023. Accessed: 2024-11-16. 1
- [23] Peixuan Li and Jieyu Jin. Time3D: End-to-end joint monocular 3D object detection and tracking for autonomous driving. In *CVPR*, pages 3885–3894, 2022. 1
- [24] Yiming Li, Dekun Ma, Ziyang An, Zixun Wang, Yiqi Zhong, Siheng Chen, and Chen Feng. V2X-Sim: Multi-agent collaborative perception dataset and benchmark for autonomous driving. *IEEE Robotics and Automation Letters*, 7(4):10914–10921, 2022. 3
- [25] Yanguang Li, Bin Huang, Zeren Chen, Yufeng Cui, Feng Liang, Mingzhu Shen, Fenggang Liu, Enze Xie, Lu Sheng, Wanli Ouyang, et al. Fast-BEV: A fast and strong bird’s-eye view perception baseline. *IEEE TPAMI*, 2024. 1
- [26] Zhenxin Li, Shiyi Lan, Jose M Alvarez, and Zuxuan Wu. BEVNeXt: Reviving dense BEV frameworks for 3D object detection. In *CVPR*, pages 20113–20123, 2024.

- [27] Zhuoling Li, Xiaogang Xu, SerNam Lim, and Hengshuang Zhao. UniMODE: Unified monocular 3D object detection. In *CVPR*, pages 16561–16570, 2024.
- [28] Tingting Liang, Hongwei Xie, Kaicheng Yu, Zhongyu Xia, Zhiwei Lin, Yongtao Wang, Tao Tang, Bing Wang, and Zhi Tang. BEVFusion: A simple and robust lidar-camera fusion framework. *NeurIPS*, 35:10421–10434, 2022. 1
- [29] Tsung-Yi Lin, Priya Goyal, Ross Girshick, Kaiming He, and Piotr Dollár. Focal loss for dense object detection. In *ICCV*, pages 2980–2988, 2017. 5
- [30] Zhiwei Lin, Zhe Liu, Zhongyu Xia, Xinhao Wang, Yongtao Wang, Shengxiang Qi, Yang Dong, Nan Dong, Le Zhang, and Ce Zhu. RCBEVDet: Radar-camera fusion in bird’s-eye view for 3D object detection. In *CVPR*, pages 14928–14937, 2024. 1
- [31] Chang Liu, Mingxu Zhu, and Cong Ma. H-V2X: A large scale highway dataset for BEV perception. In *ECCV*, pages 139–157. Springer, 2025. 2, 3
- [32] Mingyu Liu, Ekim Yurtsever, Jonathan Fossaert, Xingcheng Zhou, Walter Zimmer, Yuning Cui, Bare Luka Zagar, and Alois C Knoll. A survey on autonomous driving datasets: Statistics, annotation quality, and a future outlook. *IEEE Transactions on Intelligent Vehicles*, 2024. 1, 2
- [33] Yingfei Liu, Junjie Yan, Fan Jia, Shuailin Li, Aqi Gao, Tiancai Wang, and Xiangyu Zhang. PETRv2: A unified framework for 3D perception from multi-camera images. In *ICCV*, pages 3262–3272, 2023. 1
- [34] Ze Liu, Yutong Lin, Yue Cao, Han Hu, Yixuan Wei, Zheng Zhang, Stephen Lin, and Baining Guo. Swin Transformer: Hierarchical vision transformer using shifted windows. In *ICCV*, pages 10012–10022. IEEE, 2021. 8
- [35] Zhijian Liu, Haotian Tang, Alexander Amini, Xinyu Yang, Huizi Mao, Daniela Rus, and Song Han. BEVFusion: Multi-task multi-sensor fusion with unified bird’s-eye view representation. In *Proceedings of the IEEE International Conference on Robotics and Automation (ICRA)*, pages 2774–2781. IEEE, 2023. 1, 7, 5
- [36] Zhe Liu, Jinghua Hou, Xiaoqing Ye, Tong Wang, Jingdong Wang, and Xiang Bai. SEED: A simple and effective 3D DETR in point clouds. *arXiv preprint arXiv:2407.10749*, 2024. 1
- [37] Ilya Loshchilov and Frank Hutter. SGDR: Stochastic gradient descent with warm restarts. *arXiv preprint arXiv:1608.03983*, 2016. 5
- [38] Ilya Loshchilov and Frank Hutter. Decoupled weight decay regularization. In *ICLR*, 2018. 5
- [39] Zhipeng Luo, Changqing Zhou, Gongjie Zhang, and Shijian Lu. DETR4D: Direct multi-view 3D object detection with sparse attention. *arXiv preprint arXiv:2212.07849*, 2022. 1
- [40] Yuexin Ma, Tai Wang, Xuyang Bai, Huitong Yang, Yuenan Hou, Yaming Wang, Yu Qiao, Ruigang Yang, and Xinge Zhu. Vision-centric BEV perception: A survey. *IEEE TPAMI*, 2024. 1
- [41] Yunze Man, Liang-Yan Gui, and Yu-Xiong Wang. BEV-guided multi-modality fusion for driving perception. In *CVPR*, pages 21960–21969, 2023. 1
- [42] Sambit Mohapatra, Senthil Yogamani, Heinrich Gotzig, Stefan Milz, and Patrick Mader. BEVDetNet: Bird’s-eye view lidar point cloud based real-time 3D object detection for autonomous driving. In *Proceedings of the 2021 IEEE International Intelligent Transportation Systems Conference (ITSC)*, pages 2809–2815. IEEE, 2021. 1
- [43] Oskar Natan and Jun Miura. Towards compact autonomous driving perception with balanced learning and multi-sensor fusion. *IEEE Transactions on Intelligent Transportation Systems*, 23(9):16249–16266, 2022. 1
- [44] Gerhard Neuhold, Tobias Ollmann, Samuel Rota Buló, and Peter Kotschieder. The Mapillary vistas dataset for semantic understanding of street scenes. In *ICCV*, pages 4990–4999, 2017. 3
- [45] Lang Peng, Zhirong Chen, Zhangjie Fu, Pengpeng Liang, and Erkang Cheng. BEVSegFormer: Bird’s-eye view semantic segmentation from arbitrary camera rigs. In *Proceedings of the IEEE/CVF Winter Conference on Applications of Computer Vision*, pages 5935–5943, 2023. 1
- [46] Quang-Hieu Pham, Pierre Sevestre, Ramanpreet Singh Pahwa, Huijing Zhan, Chun Ho Pang, Yuda Chen, Armin Mustafa, Vijay Chandrasekhar, and Jie Lin. A*3D dataset: Towards autonomous driving in challenging environments. In *Proceedings of the IEEE International Conference on Robotics and Automation (ICRA)*, pages 2267–2273. IEEE, 2020. 3
- [47] John Phillips, Julieta Martinez, Ioan Andrei Bârsan, Sergio Casas, Abbas Sadat, and Raquel Urtasun. Deep multi-task learning for joint localization, perception, and prediction. In *CVPR*, pages 4679–4689, 2021. 1
- [48] Stephan R Richter, Vibhav Vineet, Stefan Roth, and Vladlen Koltun. Playing for data: Ground truth from computer games. In *ECCV*, pages 102–118. Springer, 2016. 3
- [49] German Ros, Laura Sellart, Joanna Materzynska, David Vazquez, and Antonio M Lopez. The SYNTHIA dataset: A large collection of synthetic images for semantic segmentation of urban scenes. In *CVPR*, pages 3234–3243, 2016. 3
- [50] Hao Shao, Letian Wang, Ruobing Chen, Hongsheng Li, and Yu Liu. Safety-enhanced autonomous driving using interpretable sensor fusion transformer. In *Conference on Robot Learning*, pages 726–737. PMLR, 2023. 1
- [51] Kai Simon and Georg Lausen. ViPER: Augmenting automatic information extraction with visual perceptions. In *Proceedings of the 14th ACM International Conference on Information and Knowledge Management*, pages 381–388, 2005. 3
- [52] Leslie N Smith. Cyclical learning rates for training neural networks. In *2017 IEEE Winter Conference on Applications of Computer Vision (WACV)*, pages 464–472. IEEE, 2017. 5
- [53] Zhihang Song, Zimin He, Xingyu Li, Qiming Ma, RuiBo Ming, Zhiqi Mao, Huaxin Pei, Lihui Peng, Jianming Hu, Danya Yao, et al. Synthetic datasets for autonomous driving: A survey. *IEEE Transactions on Intelligent Vehicles*, 2023. 1
- [54] Pei Sun, Henrik Kretzschmar, Xerxes Dotiwalla, Aurelien Chouard, Vijaysai Patnaik, Paul Tsui, James Guo, Yin Zhou,

- Yuning Chai, Benjamin Caine, et al. Scalability in perception for autonomous driving: Waymo open dataset. In *CVPR*, pages 2446–2454, 2020. 3, 6
- [55] Tao Sun, Mattia Segu, Janis Postels, Yuxuan Wang, Luc Van Gool, Bernt Schiele, Federico Tombari, and Fisher Yu. SHIFT: A synthetic driving dataset for continuous multi-task domain adaptation. In *CVPR*, pages 21371–21382, 2022. 3
- [56] Michal Uricár, David Hurych, Pavel Krizek, and Senthil Yogamani. Challenges in designing datasets and validation for autonomous driving. *arXiv preprint arXiv:1901.09270*, 2019. 2
- [57] Haiyang Wang, Hao Tang, Shaoshuai Shi, Aoxue Li, Zhen-guo Li, Bernt Schiele, and Liwei Wang. UniTR: A unified and efficient multi-modal transformer for bird’s-eye view representation. In *ICCV*, pages 6792–6802, 2023. 1
- [58] Li Wang, Xinyu Zhang, Ziyang Song, Jiangfeng Bi, Guoxin Zhang, Haiyue Wei, Liyao Tang, Lei Yang, Jun Li, Caiyan Jia, et al. Multi-modal 3D object detection in autonomous driving: A survey and taxonomy. *IEEE Transactions on Intelligent Vehicles*, 8(7):3781–3798, 2023. 1
- [59] Xuan Wang, Kaiqiang Li, and Abdellah Chehri. Multi-sensor fusion technology for 3D object detection in autonomous driving: A review. *IEEE Transactions on Intelligent Transportation Systems*, 2023. 1
- [60] Yue Wang, Vitor Campagnolo Guizilini, Tianyuan Zhang, Yilun Wang, Hang Zhao, and Justin Solomon. DETR3D: 3D object detection from multi-view images via 3D-to-2D queries. In *Conference on Robot Learning*, pages 180–191. PMLR, 2022. 1
- [61] Yingjie Wang, Jiajun Deng, Yao Li, Jinshui Hu, Cong Liu, Yu Zhang, Jianmin Ji, Wanli Ouyang, and Yanyong Zhang. Bi-LRFusion: Bi-directional lidar-radar fusion for 3D dynamic object detection. In *CVPR*, pages 13394–13403, 2023. 1
- [62] Xinshuo Weng, Yunze Man, Jinhyung Park, Ye Yuan, Matthew O’Toole, and Kris M Kitani. All-in-One Drive: A comprehensive perception dataset with high-density long-range point clouds. *OpenReview submission*, 2023. 3, 6
- [63] Benjamin Wilson, William Qi, Tanmay Agarwal, John Lambert, Jagjeet Singh, Siddhesh Khandelwal, Bowen Pan, Ratnesh Kumar, Andrew Hartnett, Jhony Kaesemodel Pontes, et al. Argoverse 2: Next generation datasets for self-driving perception and forecasting. *arXiv preprint arXiv:2301.00493*, 2023. 3, 6
- [64] Enze Xie, Zhiding Yu, Daquan Zhou, Jonah Philion, Anima Anandkumar, Sanja Fidler, Ping Luo, and Jose M Alvarez. M²BEV: Multi-camera joint 3D detection and segmentation with unified bird’s-eye view representation. *arXiv preprint arXiv:2204.05088*, 2022. 1
- [65] Kaixin Xiong, Shi Gong, Xiaoqing Ye, Xiao Tan, Ji Wan, Errui Ding, Jingdong Wang, and Xiang Bai. CAPE: Camera view position embedding for multi-view 3D object detection. In *CVPR*, pages 21570–21579, 2023.
- [66] Weiyi Xiong, Jianan Liu, Tao Huang, Qing-Long Han, Yuxuan Xia, and Bing Zhu. LXL: Lidar excluded lean 3D object detection with 4D imaging radar and camera fusion. *IEEE Transactions on Intelligent Vehicles*, 2023. 1
- [67] Danfei Xu, Dragomir Anguelov, and Ashesh Jain. PointFusion: Deep sensor fusion for 3D bounding box estimation. In *CVPR*, pages 244–253. IEEE, 2018. 1
- [68] Runsheng Xu, Hao Xiang, Xin Xia, Xu Han, Jinlong Li, and Jiaqi Ma. OPV2V: An open benchmark dataset and fusion pipeline for perception with vehicle-to-vehicle communication. In *Proceedings of the International Conference on Robotics and Automation (ICRA)*, pages 2583–2589. IEEE, 2022. 3, 5
- [69] Runsheng Xu, Zhengzhong Tu, Hao Xiang, Wei Shao, Bolei Zhou, and Jiaqi Ma. CoBEVT: Cooperative bird’s-eye view semantic segmentation with sparse transformers. In *Conference on Robot Learning*, pages 989–1000. PMLR, 2023. 1
- [70] Chenyu Yang, Yuntao Chen, Hao Tian, Chenxin Tao, Xizhou Zhu, Zhaoxiang Zhang, Gao Huang, Hongyang Li, Yu Qiao, Lewei Lu, et al. BEVFormer v2: Adapting modern image backbones to bird’s-eye view recognition via perspective supervision. In *CVPR*, pages 17830–17839, 2023. 1
- [71] Fisher Yu, Haofeng Chen, Xin Wang, Wenqi Xian, Yingying Chen, Fangchen Liu, Vashisht Madhavan, and Trevor Darrell. BDD100K: A diverse driving dataset for heterogeneous multitask learning. In *CVPR*, pages 2636–2645, 2020. 3
- [72] Bo Zhang, Jiakang Yuan, Botian Shi, Tao Chen, Yikang Li, and Yu Qiao. Uni3D: A unified baseline for multi-dataset 3D object detection. In *CVPR*, pages 9253–9262, 2023. 1
- [73] Jingyuan Zhao, Wenyi Zhao, Bo Deng, Zhenghong Wang, Feng Zhang, Wenxiang Zheng, Wanke Cao, Jinrui Nan, Yubo Lian, and Andrew F Burke. Autonomous driving system: A comprehensive survey. *Expert Systems with Applications*, page 122836, 2023. 1
- [74] Tianhao Zhao, Yongcan Chen, Yu Wu, Tianyang Liu, Bo Du, Peilun Xiao, Shi Qiu, Hongda Yang, Guozhen Li, Yi Yang, et al. Improving bird’s-eye view semantic segmentation by task decomposition. In *CVPR*, pages 15512–15521, 2024. 1
- [75] Xiao Zhao, Xukun Zhang, Dingkan Yang, Mingyang Sun, Mingcheng Li, Shunli Wang, and Lihua Zhang. MaskBEV: Towards a unified framework for BEV detection and map segmentation. In *ACM MM*, pages 2652–2661, 2024. 1
- [76] Benjin Zhu, Zhengkai Jiang, Xiangxin Zhou, Zeming Li, and Gang Yu. Class-balanced grouping and sampling for point cloud 3D object detection. *arXiv preprint arXiv:1908.09492*, 2019. 7
- [77] Zhuangwei Zhuang, Rong Li, Kui Jia, Qicheng Wang, Yuanqing Li, and Mingkui Tan. Perception-aware multi-sensor fusion for 3D lidar semantic segmentation. In *ICCV*, pages 16280–16290. IEEE, 2021. 1